

Section 4

**Parameterization of important
atmospheric and surface processes,
effects of different parameterizations**

Moist-entropic vertical adiabatic lapse rates: the standard cases and some lead towards inhomogeneous conditions.

Jean-François Geleyn¹ and Pascal Marquet²

¹ CNRM, Météo-France, Toulouse, France – jean-francois.geleyn@meteo.fr

² DPrévi/Labo, Météo-France, Toulouse, France

In a recent paper, Marquet (2011) proposed a new moist-entropic potential temperature θ_s , linked to the second law of thermodynamics through its full equivalence to the specific moist entropy s , i.e. with consideration of the ‘dry air’ and ‘water species’ subparts of the atmospheric parcel, of specific content q_d plus the total water specific content $q_t = 1 - q_d = q_v + q_l + q_i$. The likely advantage of θ_s with respect to earlier proposals is that it is both Lagrangian-conservative and tractable in mixing processes. Given the obvious links between any kind of potential temperature and vertical adiabatic lapse rates, we elected to do the analytical computation of such lapse rates on the basis of parcels keeping θ_s constant. This can be done without approximation only for the cases (i) of no condensed phase at all (named here ‘non-saturated’, rather than using the ambiguous ‘dry’) and (ii) of fully saturated conditions (named here ‘saturated’). Beware that we shall consider here only saturation with respect to liquid water, the extension to ice water conditions being rather straightforward. In fact the results presented below were obtained with the even more ambitious goal to look at the vertical stability under any (neutral or not) conditions, see Marquet and Geleyn (2012). But we shall concentrate here on the adiabatic lapse rates, going for this to further details than in the above-mentioned paper.

Despite the apparent complexity of the analytical formulation for θ_s ,

$$\theta_s = T \left(p_0 / p \right)^{R_d / c_{pd}} e^{-\left(\frac{L_{vap}(T) q_l}{c_{pd} T} \right)} e^{(\Lambda_r q_t)} \left(\frac{T}{T_r} \right)^{\lambda q_t} \left(\frac{p}{p_r} \right)^{-\kappa \delta q_t} \left(\frac{r_r}{r_v} \right)^{\gamma q_t} \\ \times \frac{(1 + \eta r_v)^{\kappa(1 + \delta q_t)}}{(1 + \eta r_r)^{\kappa \delta q_t}},$$

the results in terms of adiabatic lapse rates are beautifully compact. Indeed, the formulations (11) and (16) to (18) in Marquet and Geleyn (2012) can be written as:

- in the non-saturated case $\Gamma_{ns} = g / c_p$;

$$\text{- in the saturated case } \Gamma_{sw} = (g / c_p) \frac{1 + \left(\frac{L_{vap}(T) r_{sw}}{R_d T} \right)}{1 + \left(\frac{R}{c_p} \right) \left(\frac{L_{vap}(T)}{R_v T} \right) \left(\frac{L_{vap}(T) r_{sw}}{R_d T} \right)}.$$

The first formulation, with c_p obviously depending on the parcel’s composition (q_d, q_v, q_l, q_i), was expected. But the second one differs from the ‘classical’ ones advocated by Durran and Klemp (1982) or Emmanuel (1994), which both contain an additional term in the lower case

and do not return to g/c_p when eliminating the aspects linked to condensation. Probably because of the very general character of θ_s , our saturated result on the contrary allows identifying as sole specific multipliers, the non-saturated adiabatic lapse rate, the ‘full parcel kappa’ R/c_p and the Clausius-Clapeyron factor. The results thus sound logical and especially consistent, since they take into account in a fully logical way the dependence of L_{vap} , c_p and R with the temperature and composition of the moist air.

Now, if trying to get away from our extreme cases (non-saturated and saturated), one notices that, owing to their simplicity, the transition between both formulations is equivalent to just replacing the constant “ I ” by $(R/c_p) [L_{vap} / (R_v T)]$. But the second value may also be reorganised in the shape $[L_{vap}/(c_p T)] / (R_v/R)$. The latter expression is nothing else (Marquet and Geleyn, 2012, Appendix F) than the ratio of the impacts of water vertical transport on buoyancy, between saturated conditions (when only latent heat release acts) and non-saturated conditions (when only density-linked expansion acts).

Hence, defining by C a weighting factor (which may, in a certain sense, be considered as the proportion of an air parcel being in saturated conditions), it is natural to express a generalised shape for the vertical adiabatic lapse rate, now under non-homogeneous conditions:

$$F(C) = 1 + C \left[\frac{L_{vap}(T) R}{c_p T R_v} - 1 \right], \quad D_C = \frac{L_{vap}(T) r_{sw}}{R_d T}, \quad r_{sw} = \frac{\varepsilon e_{sw}(T)}{p - e_{sw}(T)},$$

$$\Rightarrow \boxed{\Gamma(C) = (g / c_p) \frac{1 + D_C}{1 + F(C) D_C} .}$$

Two remarks are needed here:

- Alike in the above-mentioned earlier publications, our definition of the saturation point corresponds to reversible conditions (i.e. at constant q_t) and not to the irreversible ones of ‘permanent exact saturation’. In the second case it is q_{sw} which would depend only on pressure and temperature, in the first case this happens for r_{sw} .
- If D_C had been written with r_v replacing r_{sw} , $\Gamma(C)$ would still have been compatible with its two extreme boundary conditions. But it is precisely in order to get the more logical situation of a term independent of the air parcel’s composition multiplying $F(C)$ that we chose the above D_C formulation for $\Gamma(C)$, expressed in terms of r_{sw} .

Concerning the second remark, one may even make D_C more compact with the help of the Clausius-Clapeyron relationship:

$$D_C = \frac{L_{vap}(T)}{R_v T} \left[\frac{e_{sw}(T)}{p - e_{sw}(T)} \right] = \frac{T}{p - e_{sw}} \frac{de_{sw}}{dT} !$$

Most of this work was performed in the framework of the EU-ESF COST ES0905 action.

References:

- Durrant, DR. and JB. Klemp, 1982. *J. Atmos. Sci.*, **39**, pp. 2152-2158.
 Emanuel, KA., 1994. Atmospheric convection. *Oxford University Press*.
 Marquet, P., 2011. *Q. J. R. Meteorol. Soc.*, **137**, pp. 768-791.
 Marquet, P. and J.-F. Geleyn, 2012. To appear in *Q. J. R. Meteorol. Soc.*.

Effects of atmospheric planetary and surface boundary-layer schemes on simulations of intense tropical cyclones

Sachie Kanada¹ and Akiyoshi Wada²

¹Japan Agency for Marine-Earth Science and Technology, 1-1 Nagamine, Tsukuba, Ibaraki 305-0052, Japan

²Meteorological Research Institute/JMA, Japan

skanada@mri-jma.go.jp

1 Introduction

A simulation of the development of tropical cyclones (TCs) is strongly affected by atmospheric planetary and surface boundary-layer schemes. In this study, the sensitivity experiments are conducted for an intense TC by using a nonhydrostatic atmospheric model [Saito et al., 2007] with a horizontal resolution of 2 km (NHM2). The planetary boundary layer (PBL) schemes used in this study are the Mellor–Yamada–Nakanishi–Niino (MYNN) scheme [Nakanishi and Niino, 2004]: level 3 (‘CNTL2’ or no index in Table 1) and the Deardorff–Blackadar scheme (‘dd’ in Table 1), respectively. The surface boundary schemes are Beljaars and Holtslag [1991] (‘H’ in Table 1) and Louis et al. [1982] (‘L’ in Table 1), respectively. Beljaars [1994] (‘B’ in Table 1) and Kondo [1975] (‘K’ in Table 1) are used for calculating the surface roughness length (z_0).

2 Model descriptions

The computational domains covered an area of 2600 km × 2400 km, centered at 22.5°N, 142.5°E with 50 vertical levels with variable height, from 40 m for the lowermost layer near the surface to 904 m for the uppermost layer. The top height was approximately 22 km. The boundary conditions including sea surface temperature were provided every 6 hours from the experiment by an atmospheric general circulation model with a horizontal resolution of 20km [AGCM20, Mizuta et al., 2012]. The integration period was 6 days from 0600 UTC, 16 September 1983, which targeted a TC (MCP, 866 hPa) simulated by AGCM20, that was the most intense at 0600 UTC on 21 September. Detail of the model descriptions are summarized in Kanada et al. [2012].

3 Results

Figure 1 clearly shows differences in the central pressure (CP) evolution between experiments in Table 1. Minimum CP (MCP) was 916 hPa in CNTL2, 886 hPa in 2HK, 914 hPa in 2LB, 888 hPa in 2LK, 910 hPa in 2dd, and 877 hPa in 2ddLK (Table 1). Regardless of the PBL and surface boundary schemes, all K-experiments (2HK, 2LK and 2ddLK) showed rapid intensification exceeding 30 hPa day⁻¹ and have MCPs lower than 890 hPa. On the

other hand, all B-experiments (CNTL2, 2LB and 2dd) gradually developed, and had MCPs higher than 910 hPa. These results indicate the largest impact of the z_0 -settings on the development of TC in the experiments. Little difference was found between H- and L-experiments (See CNTL2 and 2LB, and 2HK and 2LK). CPs in dd-experiments developed more rapidly than those in MYNN-experiments (See CNTL2 and 2dd, and 2LK and 2ddLK). Note that AGCM20 which attained the lowest MCP of 866 hPa, did not show the rapid intensification.

Table 1 List of control and sensitivity experiments [PBL, surface boundary schemes and surface roughness length (z_0)]

Experiment	PBL and surface schemes
CNTL2 (2HB)	Mellor-Yamada-Nakanishi-Niino Level 3 [Nakanishi and Niino, 2004] / Beljaars and Holtslag [1991] / Beljaars [1994]
2HK	Mellor-Yamada-Nakanishi-Niino Level 3 [Nakanishi and Niino, 2004] / Beljaars and Holtslag [1991] / Kondo [1975]
2LB	Mellor-Yamada-Nakanishi-Niino Level 3 [Nakanishi and Niino, 2004] / Louis et al. [1982] / Beljaars [1994]
2LK	Mellor-Yamada-Nakanishi-Niino Level 3/ [Nakanishi and Niino, 2004] / Louis et al. [1982] / Kondo [1975]
2dd	Deardorff[1980], Blackadar[1962] / Beljaars and Holtslag [1991] / Beljaars [1994]
2ddLK	Deardorff[1980], Blackadar[1962] / Louis et al. [1982] / Kondo [1975]

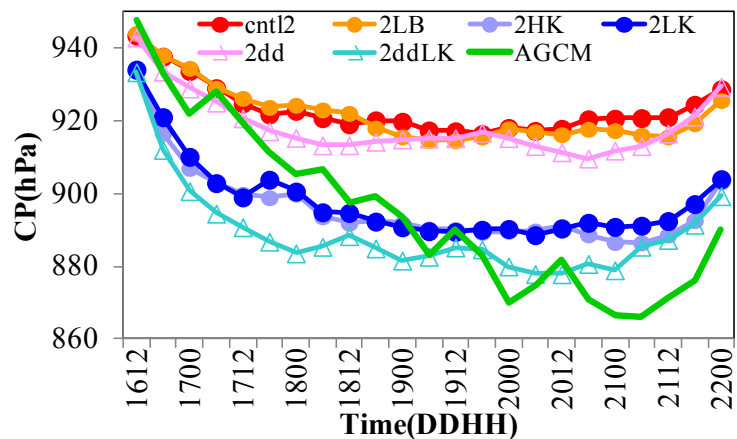


Figure 1 Time variation of CP.

The distributions of hourly precipitation amounts showed differences between the MYNN- and dd-experiments (Figure 2). At the most intense phase, a region of moderate precipitation exceeding 10 mm h^{-1} widely expanded on the eastern side of the TC center in MYNN-experiments (CNTL2 and LK: Figures 2a and 2c). On the other hand, a region of precipitation was relatively small in dd-experiments (2dd and 2ddLK: Figures 2b and 2d) and a region of intense precipitation exceeding 70 mm hr^{-1} concentrated around the inner-core. Radial profiles of 24-hourly mean azimuthally averaged winds revealed that large radial winds (V_r ; inflow is represented by a positive value) exceeding 20 m s^{-1} were found in dd-experiments regardless of the values of MCP (Figure 3d), while those in MYNN-experiments were smaller than 20 m s^{-1} . Tangential winds (V_t) were sensitive to the setting of z_0 (Figure 3c).

4 Summary and Remarks

Our results indicate that both the PBL and the surface roughness length (z_0) have a large impact on the structure and the development of an intense tropical cyclone (TC). The settings of z_0 have the largest impact on the rapid intensification of the simulated TC. In addition, differences among the experiments with two PBL schemes are found in the CP evolutions, horizontal distributions of precipitation and wind fields. Further analysis is required to study the essential factors for the development of an intense TC.

References

- Beljaars, A.C.M., 1994: The parameterization of surface fluxes in large-scale models under free convection. *Quart. J. Roy. Meteor. Soc.*, 121, 255–270.
- Beljaars, A.C.M. and A.A.M. Holtslag, 1991: Flux parameterization over land surfaces for atmospheric models. *J. Appl. Meteor.*, 30, 327–341.
- Kanada, S., A. Wada, M. Nakano, and T. Kato, 2012: Effect of PBL schemes on the development of intense tropical cyclones using a cloud resolving model. *J. Geophys. Res.*, 117, D03107, doi:10.1029/2011JD016582.
- Kondo, J., 1975: Air-sea bulk transfer coefficients in diabatic conditions. *Bound.-Layer Meteor.*, 9, 91–112.
- Louis, J.F., M. Tiedtke, and J.F. Geleyn, 1982: A short history of the operational PBL parameterization at ECMWF. *Proc. Workshop on Planetary Boundary Layer Parameterization*, Reading, United Kingdom, ECMWF, 59–79.
- Mizuta, R., H. Yoshimura, H. Murakami, M. Matsueda, H. Endo, T. Ose, K. Kamiguchi, M. Hosaka, M. Sugi, S. Yukimoto, S. Kusunoki and A. Kitoh, 2012: Climate simulations using MRI-AGCM3.2 with 20-km grid. *J. Meteor. Soc. Japan*, in press.
- Nakanishi, M. and H. Niino, 2004: An improved Mellor-Yamada level 3 model with condensation physics: Its design and verification. *Bound.-Layer Meteor.*, 112, 1–31.
- Saito, K., J. Ishida, K. Aranami, T. Hara, T. Segawa, M. Narita, and Y. Honda, 2007: Nonhydrostatic atmospheric models and operational development

at JMA. *J. Meteor. Soc. Japan*, 85B, 271–304.

Acknowledgment

This study was supported by the Ministry of Education, Culture, Sports, Science and Technology of Japan under the framework of the Kakushin Program. Numerical simulations were performed using the Earth Simulator. A. Wada was supported by the Japan Society for the Promotion of Science (JSPS), Grant-in-Aid for Scientific Research (C) (22540454).

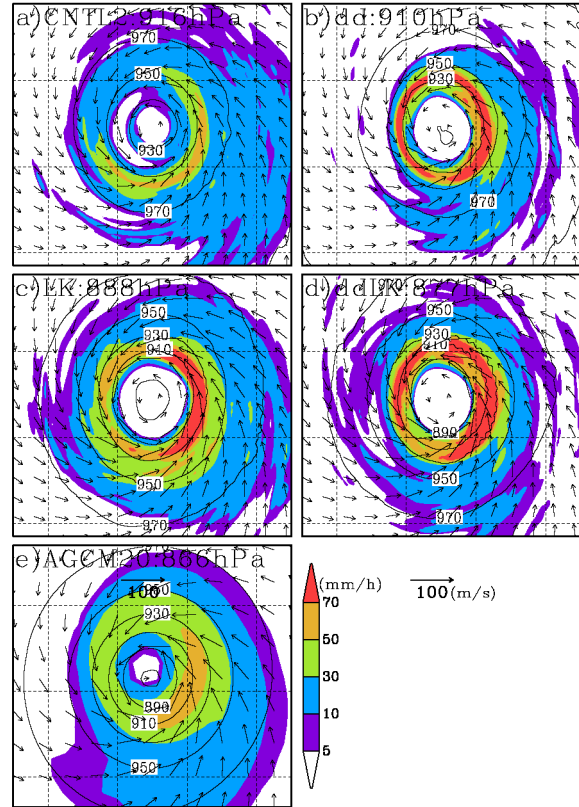


Figure 2 Horizontal distributions of hourly precipitation amounts in the 1 h preceding the most intense phase of the TC: a) CNTL2, b) 2dd, c) 2LK, d) 2ddLK and e) AGCM20. The MCP is indicated in each panel. Arrows indicate 10 m level winds.

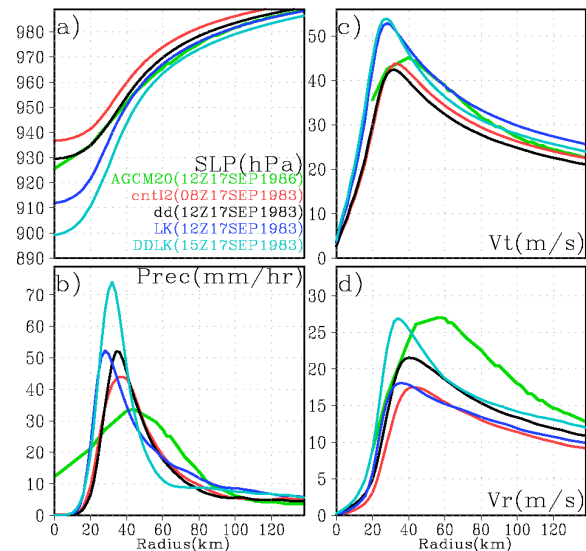


Figure 3 Radial profiles of 24-hourly mean azimuthally averaged a) sea level pressure, b) precipitation, c) tangential wind and d) radial wind speed at a height of 10 m during the rapid intensification phase. AGCM20: green, CNTL2: red, 2dd: black, 2LK: blue, 2ddLK: cyan.

The impact of a non-orographic gravity wave drag parameterization scheme on the middle atmosphere in JMA's Global Spectral Model

Takafumi Kanehama

Numerical Prediction Division, Japan Meteorological Agency

e-mail: tkanehama@met.kishou.go.jp

1. Introduction

The Japan Meteorological Agency (JMA) plans to raise the top level of its operational Global Spectral Model (GSM) from 0.1 hPa to 0.01 hPa to include the whole stratosphere and place a model lid on the mesopause. The total number of vertical layers will be increased from 60 to 100 according to the tentative plan. One of the aims of these developments is to improve the representation of the middle atmosphere (i.e., the stratosphere and mesosphere), where gravity waves play a key role as a driving force for meridional circulation and long-term oscillations such as QBO (quasi-biennial oscillation). As gravity waves have smaller horizontal and vertical scales than the model's resolutions, their effects need to be parameterized in the GSM. To this end, a non-orographic gravity wave drag scheme [1] was tested in the vertically extended GSM.

2. Experiment Configuration

A six-year integration was conducted for the period 1995 – 2000 to clarify the impact of the non-orographic gravity wave drag scheme with the vertically extended low-horizontal-resolution GSM TL95L100. The model physics used were the same as those of the operational GSM in the control experiment (hereafter referred to as CNTL). In the test experiment (hereafter referred to as TEST), Rayleigh friction in the current operational GSM was replaced with the non-orographic gravity wave drag scheme. The parameters of the test scheme were different from those described in the original paper.

3. Results

Figure 1 shows zonally averaged zonal winds in the tropical lower stratosphere. Compared to ERA-Interim data [2], the TEST experiment outcome successfully shows QBO-like periodic changing zonal winds. However, the period is shorter than that of ERA-Interim. Additionally, the amplitude of the westerly wind phase is over 10 ms^{-1} weaker. No signs of QBO were captured in the CNTL experiment.

Model climatologies for zonal mean temperature and zonal wind fields in January are shown in Figure 2. Compared to the SPARC [3] climatology, the weak easterly jet bias in the middle atmosphere of the summer hemisphere in CNTL was alleviated in TEST. However, both experiments failed to reproduce the closed structure of the westerly jet in the mesosphere. In addition, temperatures in the upper mesosphere were over 20 K warmer than those of SPARC. The main cause of this bias is the excessive mesospheric ozone climatology used in the short-wave radiation scheme. Although the upper mesosphere in summer is cooler than the lower mesosphere in winter for SPARC, neither experiment reproduced such a structure. This suggests that both experiments were unable to represent meridional circulation leading to upward (downward) motion of the air producing adiabatic cooling (heating) in the summer upper (winter lower) mesosphere. The climatologies for July have features similar to those for January (not shown) even though the seasons are opposite.

The results described here are preliminary in nature, and further investigation is being conducted by

NPD/JMA. Some parameters of the non-orographic gravity wave drag scheme in TEST are also being tuned to improve its representation of the middle atmosphere in consideration of the accuracy and biases of other parameterizations such as long- and short-wave radiation schemes.

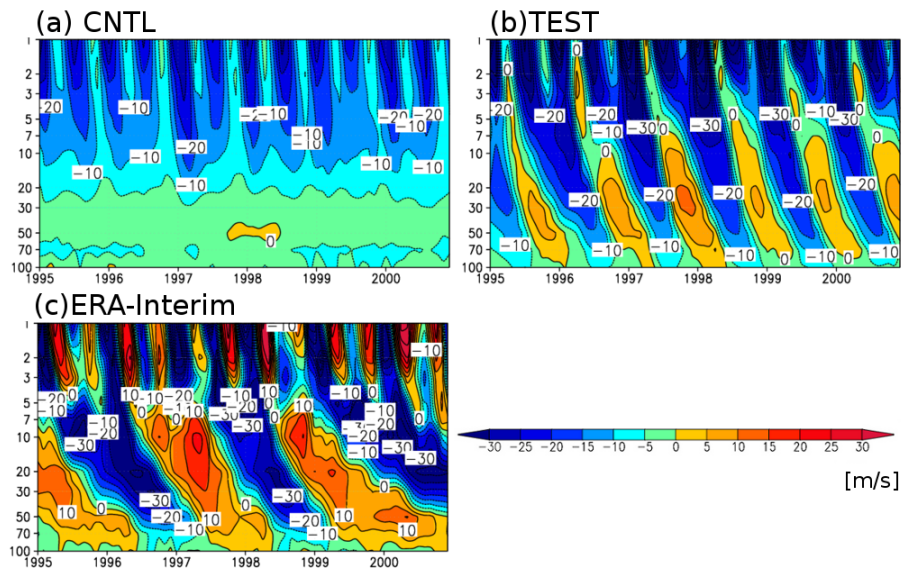


Figure 1. Time evolution of zonally averaged zonal winds (ms^{-1}) averaged over the $5^{\circ}\text{S} - 5^{\circ}\text{N}$ region. Positive values indicate westerly winds. (a) Control experiment: TL95L100 with Rayleigh friction; (b) test experiment: TL95L100 with a non-orographic gravity wave drag scheme; (c) ERA-Interim.

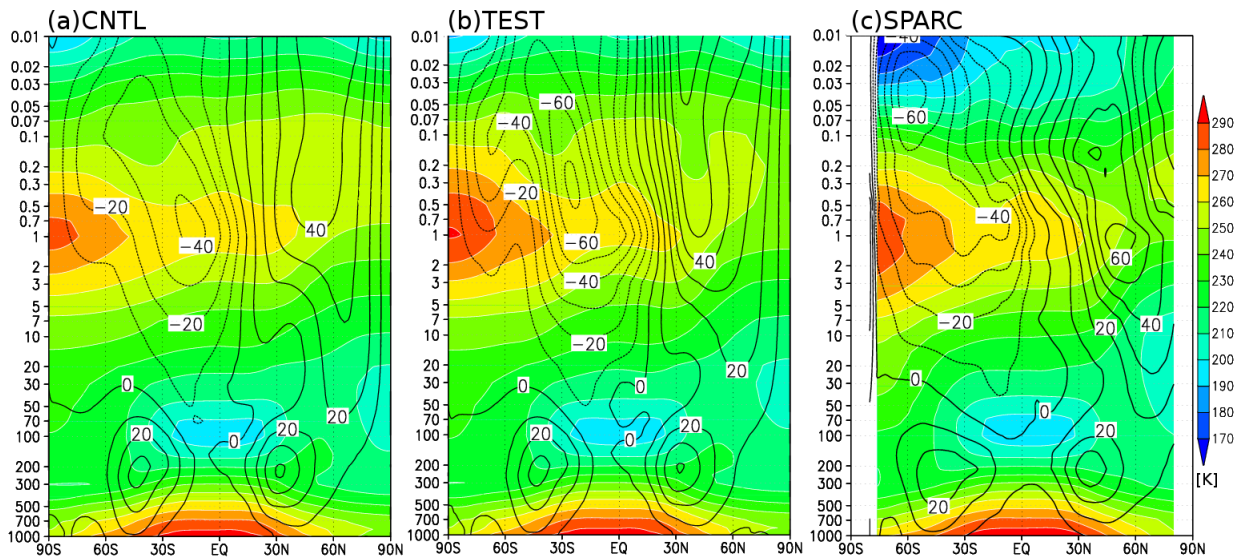


Figure 2. Zonal mean climatologies of zonal wind (contours, ms^{-1}) and temperature (shaded, K) for January. The contour intervals are 10 m/s . (a) Control experiment: TL95L100 with Rayleigh friction; (b) test experiment: TL95L100 with a non-orographic gravity wave drag scheme; (c) SPARC climatology. SPARC climatology for the $90^{\circ}\text{S} - 75^{\circ}\text{S}$ and $80^{\circ}\text{N} - 90^{\circ}\text{N}$ regions is not shown due to a lack of data.

References

- [1] Scinocca, J. F., 2003: An accurate spectral nonorographic gravity wave drag parameterization for general circulation models. *J. Atmos. Sci.*, **60**, 667 – 682.
- [2] Dee, D. P. et al., 2011: The ERA-Interim reanalysis: configuration and performance of the data assimilation system. *Quart. J. Roy. Meteor. Soc.*, **137**, 553 – 597.
- [3] Randel, W. et al., 2004: The SPARC intercomparison of middle-atmosphere climatologies. *J. Climate*, **17**, 986 –

Dependency of horizontal and vertical resolutions, and turbulence schemes on snowfall forecasts: Part II Differences of vertical profiles

Teruyuki KATO

Japan Meteorological Agency/Meteorological Research Institute, Chiyoda-ku, Tokyo, Japan
(E-mail: tkato@mri-jma.go.jp)

1. Introduction

Kato (2011) reported that the dependency of horizontal resolutions (500 m - 5 km) and vertical ones, and turbulence schemes (Mellor-Yamada level 3 (Nakanishi and Niino 2006): MYNN, Deardroff (1980): DD) on snowfall forecast, by using the Japan Meteorological Agency (JMA) nonhydrostatic model (Saito et al. 2007), and showed in comparison with the 1km-model with DD that MYNN increased sensitive and latent heat fluxes through the enhancement of low-level wind speeds, while it decreased snowfall amounts. In this study, the reason is examined from the stratification of lower atmosphere and the vertical profiles of updrafts and cloud water amounts.

2. Experimental designs

At first, 12-hour forecasts for a domain shown in Fig. 1a are conducted every 6 hours during 16-20 December 2009 by the 5km-model whose initial and boundary conditions are produced from 6-hourly available JMA mesoscale analyses with a horizontal resolution of 5 km. Then, 9-hour forecasts with 2km-, 1km- and 500m-models for a domain shown in Fig. 1b are conducted by driving the 3-hour to 12-hour forecasts of the 5km-model. Verification datasets for 5 days are produced from hourly output of last 6-hour forecasts of each model. Statically analyses are made for an area shown in the red rectangle in Fig. 1b.

A bulk-type microphysics parameterization scheme in which two moments are treated only for ice hydrometeors (i.e., snow, graupel and cloud ice) is used for precipitation processes in all models, and the Kain-Fritsch convection parameterization scheme is additionally used in the 5km-model. In comparison with control simulations (50 vertical layers), the simulation with 70 vertical layers has about a half vertical resolution below a height of 3 km.

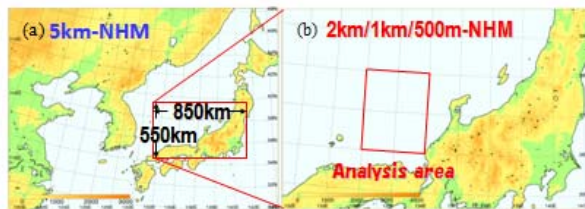


Fig. 1 Model domain and topography of (a) 5km-model and (b) 1km-model. The domains of 2km- and 500m-models are the same as (b).

3. Differences of 1km-NHM results between MYNN and Deardroff

Table 1 shows 5-day mean values in 1km-models

with MYNN (dx01) and DD (dx01_dd) averaged within the red rectangle in Fig. 1b. The latent heat flux is about 20 % larger in dx01 than in dx01_dd, while the precipitation amount is about 8 % smaller. The larger values of latent and sensitive fluxes in dx01 are mainly caused by about 16 % larger values of the maximum and mean horizontal speeds for dx01_dd. The difference of specific humidity between the lowest model layer and the sea surface (Δq_v) is larger in dx01 than in dx01_dd, while that of potential temperature (ΔPT) is smaller. This causes that the ratio (dx01/dx01_dd) of sensitive heat flux (11%) becomes smaller than that of latent heat flux. These differences indicate that MYNN immediately transports water vapor upward to decrease its amounts remained near the surface.

Table 1 also shows that the difference of precipitation between dx01 and dx01_dd is almost brought from that of graupel. Since strong updrafts and lots of cloud water are necessary for the production of graupel, it can be supposed that cloud water amounts are less in MYNN than in DD and updrafts are weaker.

Table 1 Five-day mean values in 1km-models with MYNN (dx01) and DD (dx01_dd) averaged within the red rectangle in Fig. 1b. The ratio means dx01/dx01_dd, and SHflux indicates sensitive heat flux, LHflux latent heat flux, MaxWind the maximum horizontal wind speed, MeanWind mean horizontal wind speed. ΔPT and Δq_v indicate the differences of potential temperature and specific humidity between the lowest model layer and the sea surface, respectively.

	dx01	dx01_dd	ratio
SHflux (W/s)	214.1	193.2	1.11
LHflux (W/s)	346.1	288.2	1.20
MaxWind (m/s)	20.93	18.83	1.11
MeanWind (m/s)	13.08	11.29	1.16
MeanWind (m/s)	13.08	11.29	1.16
ΔPT (K)	13.07	13.46	0.97
Δq_v (g/kg)	8.27	7.85	1.05
Precipitation (mm)	39.15	42.65	0.92
Rain (mm)	10.42	10.73	0.97
Snow (mm)	21.73	21.09	1.03
Graupel (mm)	7.00	10.83	0.65

4. Vertical profiles in the lower atmosphere

Five-day mean vertical profiles of virtual potential temperature (Fig. 2) shows that the classification can be made by turbulent scheme, not horizontal resolutions. In DD an absolute unstable layer is found below a height of 200 m, while in MYNN a neutral layer is produced below a height of 500 m. Such an absolute

unstable layer is often observed over the Sea of Japan in winter. This indicates that vertical mixing is too strong in MYNN. Moreover, both DD and MYNN produce almost the same vertical profile above a height of 1500 m, but near-surface temperature becomes 0.3 K higher in MYNN than in DD. This is mainly caused by the difference of sensitive heat flux (Table 1).

Figure 3 shows the appearance frequency of lapse rates of virtual potential temperature simulated by 1km-models with MYNN and DD. Absolute unstable layers are scarcely found in MYNN, and most of lapse rates are nearly 0 K km⁻¹ below a height of 500 m. In DD, the peak height of the appearance frequency of absolute unstable layers (~ 100 m) is lower than mean values (blue line in Fig. 3b), and unstable layers due to the condensation extend to a height of 4.5 km. The latter produces buoyancy to cause the moist convection. Meanwhile, the strength of absolute instability is considerably smaller in MYNN than in DD. This means that MYNN releases most of the instability by itself. It should be noted that top heights of convective mixing layers in MYNN are almost the same as that in DD, which is independent of horizontal resolutions (not shown).

5. Vertical profiles of vertical velocity and cloud water

The vertical profile of strong updrafts (Fig. 4a) also shows that the classification can be made by turbulent schemes (MYNN and DD), except for simulations with 70 layers. The maximum of strong updrafts is found around a height of 1.1 km in DD, while the height shifts 500 m upward in MYNN. These correspond to the peak heights of the appearance frequency of absolute unstable layers (Fig. 3). In the simulations with 70 layers, updrafts weaken and the heights of strong updrafts extend vertically.

In the vertical profiles of cloud water amounts (Fig. 4b), a peak is found corresponding to the heights with the maximum updraft (Fig. 4a), and it is about 20 % larger in MYNN than in DD while such a difference is not found in strong updrafts. Larger production of cloud water in DD, which is made by larger condensation due to lower temperature (Fig. 2), could

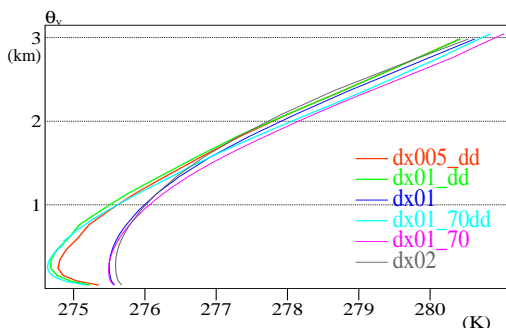


Fig. 2 Vertical profiles of 5day-mean virtual potential temperature θ_v , averaged within the red rectangle in Fig. 1b. The results of 2km-, 1km- and 500m-models are indicated by dx02, dx01 and dx005, respectively. Additional symbol of ‘_dd’ indicates the results with DD, and the others those with MYNN. The symbol of ‘70’ also indicates the results with 70 vertical layers.

cause the effective formation of graupel to bring larger snowfall amounts, in addition to strong updrafts.

References

- Kato, T., 2011: Dependency of horizontal and vertical resolutions, and turbulence schemes on snowfall forecasts. CAS/JSC WGNE Research Activities in Atmospheric and Oceanic Modelling, 41, 3.03-3.04.
 Nakanishi, M. and H. Niino, 2006: An improved Mellor-Yamada level-3 model: Its numerical stability and application to a regional prediction of advection fog. *Bound.-Layer Meteor.*, **119**, 397-407.
 Saito, K., J. Ishida, K. Aranami, T. Hara, T. Segawa, M. Nareta, and Y. Honda, 2007: Nonhydrostatic atmospheric models and operational development at JMA. *J. Meteor. Soc. Japan*, **85B**, 271-304.

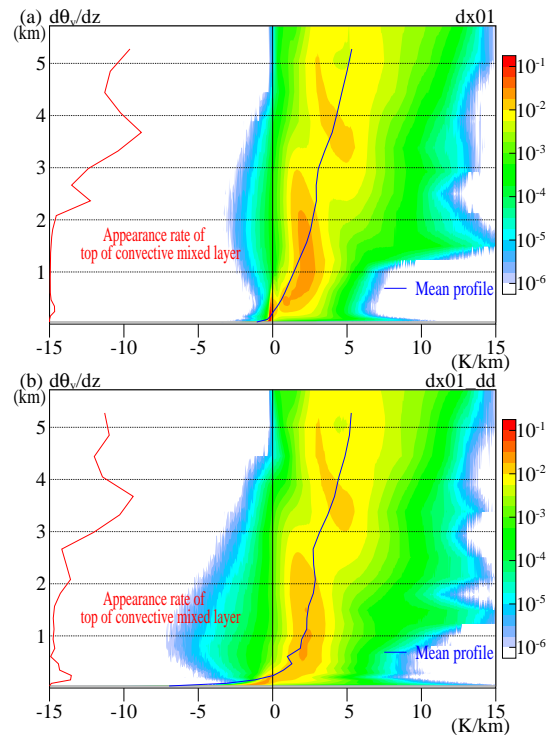


Fig.3 Same as Fig. 2, but the appearance frequency of lapse rates, simulated by 1km-models with (a) MYNN and (b) DD. Blue and red lines denote mean values and the appearance frequency of top heights of convective mixing layers, detected by $d^2\theta_v/dz^2=0$.

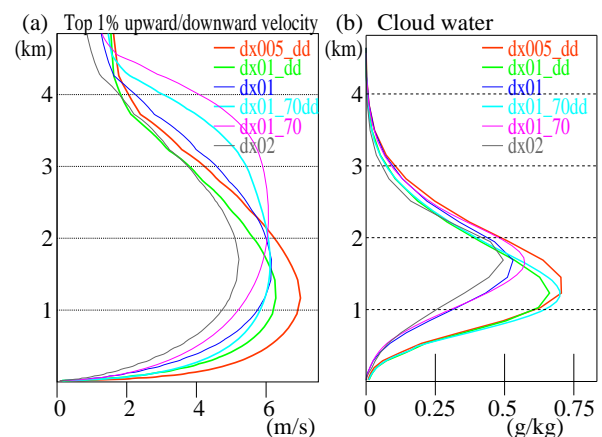


Fig. 4 Same as Fig.2, but (a) the vertical velocity of top 1% updraft and (b) the mixing ratio of cloud water.

Results of ASTEX and Composite model intercomparison cases using two versions of JMA-GSM SCM

Hideaki Kawai

Meteorological Research Institute, Japan Meteorological Agency

(e-mail: h-kawai@mri-jma.go.jp)

1. Introduction

In recent years, two model intercomparison cases have been developed to understand the transition of marine boundary layer clouds from stratocumulus (Sc) to shallow cumulus: the ASTEX Lagrangian case by Stephan de Roode, and the Composite Transition case by Irina Sandu, which is based on Sandu et al. (2010).

The cloud scheme of the operational global model of JMA (Japan Meteorological Agency), GSM (Global Spectral Model), is a PDF(Probability Density Function)-based cloud scheme (Smith 1990) and GSM also incorporates a simple Sc scheme to specifically represent Sc (Kawai and Inoue 2006). Another simple treatment for Sc is under trial to improve the vertical structure of boundary layer clouds, and solve some problems in the current operational scheme. In order to check the performance of these two versions in representing the transition of Sc to shallow cumulus, two versions of the SCM (Single Column Model) of the JMA-GSM were tested, and the results were submitted to the two intercomparison cases.

2. Two versions of JMA-GSM SCM

2.1. Sc scheme Version 1

Version 1 is the operational Sc scheme (Kawai and Inoue 2006) that was originally developed to represent Sc in models with relatively coarse vertical resolution.

The model conditions necessary to produce Sc are: (1) a strong inversion just above the layer, (2) not stable layer near the surface (to guarantee the existence of a mixed layer), and (3) application of the scheme only below 940 hPa.

When these three conditions are met, the following procedures are applied: (1) cloud cover of Sc is determined as a function of inversion strength; (2) in-cloud CWC (Cloud Water Content) is determined, as it is proportional to saturation specific humidity: $q_{cld} = \beta \cdot q_{sat}$; and (3) mixing at the top of the cloud layer is suppressed.

2.2. Sc scheme Version 2

Version 2 is a simpler scheme, but it performs reasonably well in the current GSM because of the recent increase in vertical resolution. In Version 2, the conditions needed to produce Sc are: (1) $\theta_{700} - \theta_{surf} > 20$ [K] (based on Klein and Hartmann (1993)), and (2) not stable layer near the surface. When these two conditions are met, mixing at the top of the cloud layer is completely suppressed to prevent an entrainment of dry air in free atmosphere; Additional mixing at the top of the mixed layer, which has been used in the operational model for a long time to prevent the unrealistic formation of boundary layer clouds at the top of the boundary layer, is not applied, and the lower limit of vertical diffusivity is made to be almost zero at the top of the cloud layer.

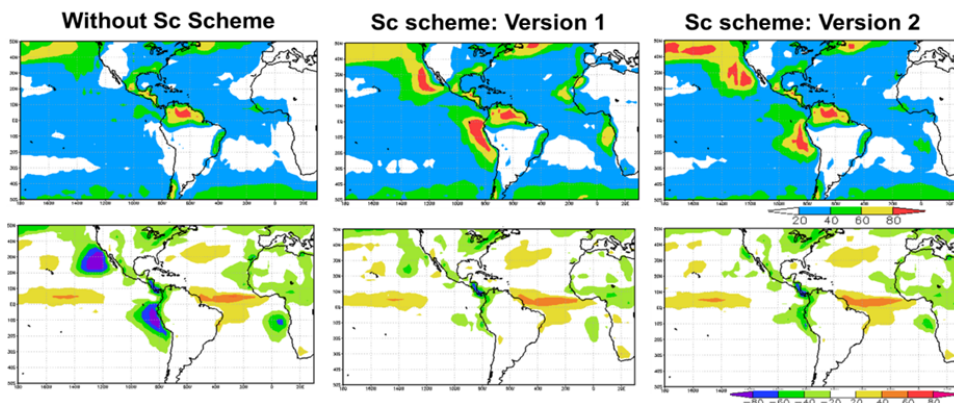


Fig. 1: Top panels: Low cloud cover (%). Lower panels: Error of TOA upward shortwave flux (W/m^2). The observation data are ERBE. Using TL159 for July calculated without an Sc scheme (left panels), with the Sc scheme version 1 (middle), and with the Sc scheme version 2 (right).

2.3. Performance of model climatology

Version 2 can produce almost the same amount of low cloud cover as Version 1, and the TOA shortwave bias of both versions is comparably small (Fig. 1), although the subtropical Sc clouds in Version 2 are slightly underestimated in areas adjacent to continents.

3. Results of the intercomparison cases

3.1. ASTEX case

In the ASTEX case, the forcing evolves from Sc circumstance into shallow cumulus circumstance. The ASTEX intercomparison case requests the calculation using a higher assigned vertical resolution, in addition to the operational resolution run. Whereas the operational GSM L60 has 13 layers lower than 2000 m, the assigned L80 resolution has 24 layers for the same range.

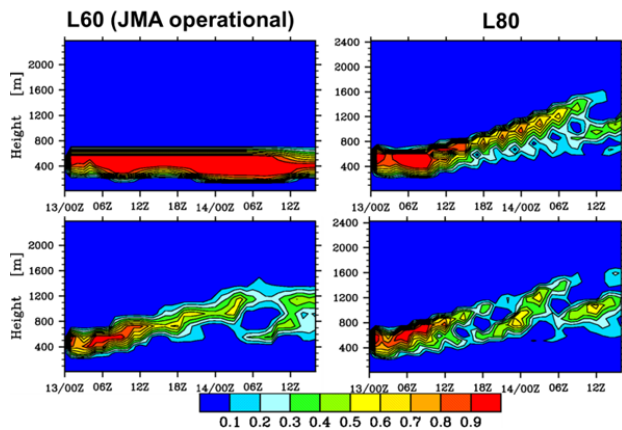


Fig. 2: Time evolution of cloud cover in the ASTEX case. Top panels correspond to Version 1 and bottom panels to Version 2, using vertical layers of the operational L60 (left), and the assigned L80 (right).

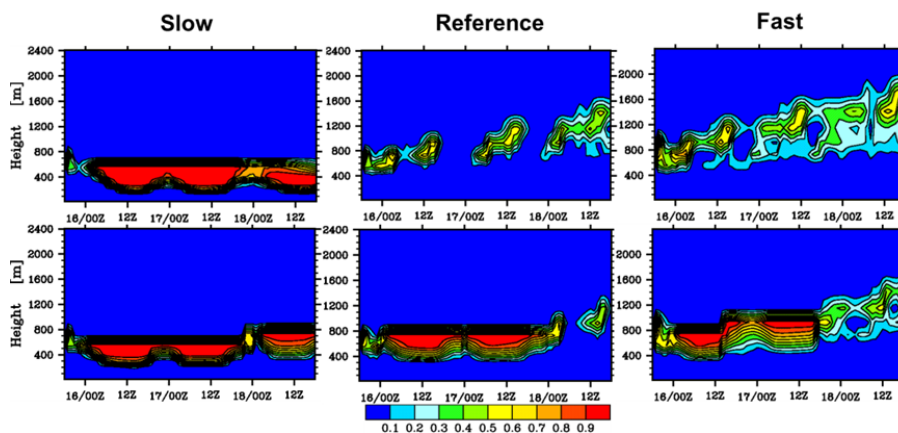


Fig. 3: Time evolution of cloud cover in the Composite case. Top panels correspond to Version 1 and bottom panels to Version 2 using slow (left), reference (middle), and fast (right) evolving forcing.

In the case of Version 1 and L60, the conditions required to produce Sc in the scheme are met throughout the simulation period, and the cloud layer remains unrealistically at the same altitude (Fig. 2). For the case of the fine resolution L80, the conditions for producing Sc are broken after several hours from the initial time. The cloud is produced by the Smith PDF scheme and the height of the cloud layer gradually increases (Fig. 2). The L80 case using Version 1 and the results using Version 2 are more consistent with observations, though the cloud cover might be not enough.

3.2. Composite case

The Composite case also gives the forcing evolving from Sc environment into shallow convection environment. Three different forcings are used in this case, which give differing speeds of the transition.

In reference forcing and fast forcing, the simulated cloud cover is too small using Version 1, because the conditions of the Sc scheme are not met (Fig. 3). On the other hand, using Version 2, the conditions are met for almost two days (Fig. 3), and the significant cloud cover for this period is similar to the LES results of many participants in this comparison. However, even when cloud amount of Sc is well represented in Version 2, the simulated height of the cloud layer is much lower than that in the LES results.

References

- Kawai, H., and T. Inoue, 2006: A simple parameterization scheme for subtropical marine stratocumulus. *SOLA*, **2**, 17–20.
- Klein, S. A., and D. L. Hartmann, 1993: The seasonal cycle of low stratiform clouds. *J. Climate*, **6**, 1587–1606.
- Sandu, I., B. Stevens and R. Pincus, 2010: On the transitions in marine boundary layer cloudiness. *Atmos. Chem. Phys.*, **10**, 2377–2391.
- Smith, R. N. B., 1990: A scheme for predicting layer clouds and their water content in a general circulation model. *Quart. J. Roy. Meteor. Soc.*, **116**, 435–460.

Evaluation from a Perspective of Spin-down Problem: Moistening Effect of Convective Parameterization

Takuya KOMORI* and Koichi YOSHIMOTO

Numerical Prediction Division, Japan Meteorological Agency, Tokyo, Japan
Email: komori@met.kishou.go.jp

1. INTRODUCTION

Model errors stem from various sources such as parameterization types and statistical sub-grid fluctuations, and basically grow from the initial state, leading to a systematic bias in model climatology. Accordingly, diagnostic measurement of short-range forecast errors before interacting globally with errors brought from unknown inherent predictability provides a wealth of beneficial information for the development of physics parameterization. Considering the differences between observations and short-range forecasts produced by the operational Global Spectral Model (GSM) highlights a problem referred to as spin-down – an issue associated with data assimilation (DA) cycles that involves a rapid decrease in humidity caused by strong precipitation during the short-range forecast period. It has been suggested that the problem is closely related to convective precipitation (Andersson et al. 2005). Against this background, the purpose of the present study was to investigate the performance of revised convection and cloud schemes in the GSM.

2. EXPERIMENTAL DESIGN

Two experiments (CNTL and TEST) were conducted to compare model performance levels. In the CNTL experiment, a low-resolution version of the operational GSM (TL319L60: 60-km horizontal resolution, 60 layers) was used. In the GSM, a convection scheme (the prognostic Arakawa-Schubert scheme with a spectral cloud ensemble) and a large-scale cloud scheme (cloud fraction is diagnosed following an assumed probability density function (PDF)) were implemented.

In the TEST experiment, a number of modifications were introduced. For the convection scheme, these were as follows: 1) the mass flux profile in the sub-cloud layers was changed in consideration of the large entrainment rate near the surface; 2) the mass flux amount was modified to vary depending on the water saturation deficit in the atmosphere; 3) the downward mass flux was reduced, starting from the Level of Free Sinking (LFS); 4) the formulation of the closure was changed from a cloud work function type to a diluting CAPE type; 5) treatment of detrained cloud water and cloud ice was modified; 6) the artificial on/off switching function for convective triggering was removed; 7) the formulation of the prognostic equation for the mass flux at the cloud base was modified; and 8) an upper limit for the cloud top was added based on calculation of the vertical velocity of an entraining parcel. For the large-scale cloud scheme, the modifications were: 1) the formulations of the PDF function were modified; and 2) the artificial threshold for low-level clouds was removed to suppress inadequate cloud data.

3. EVALUATION IN A 4D-VAR DA SYSTEM USING RETRIEVED GPS-PWV DATA

Retrieved GPS precipitable water vapor (PWV) data provides performance with a level of accuracy comparable to that of retrieved Sonde PWV data regardless of the presence or absence of rain areas. Moreover, ground-based GPS sites are located all over the world, providing a continuous stream of hourly data. GPS-PWV data are therefore useful in evaluating column water vapor and precipitation in light of the spin-down problem seen with the 4D-VAR DA system. The experiment results suggested that the problem was alleviated more in TEST than it was in CNTL (Figs. 1 and 2). In TEST, the mean error for 1 – 9 hour forecast PWV was lower, and the difference in the vertical profiles of water vapor from Sonde observations was also reduced, which related to better representation of the timing of precipitation occurrence for the short-range forecast period (not shown). These results mainly stem from the suppression of excessive deep convection during the period, with the second, seventh and eighth modifications to the convection scheme contributing significantly.

4. EVALUATION OF FORECASTS FROM 4D-VAR ANALYSIS FIELDS

The TEST forecast from the TEST analysis provided in the DA forecast cycle produced global PWV fields (Fig. 3) and lower relative humidity (RH) spin-down better than the CNTL forecast from the CNTL analysis, while RH spin-down was notable in the CNTL forecast from the TEST analysis (Fig. 4). Even if the TEST forecast starts from CNTL analysis, it does not show the same value as the TEST forecast from TEST analysis in the nine-day version. These results suggest that a consistent relationship between the initial state (analysis field) and the forecast model in the numerical weather prediction system should be elaborated. To develop moist parameterization, such evaluation in regard to the spin-down problem provides useful information for the improvement of hydrological forecasting in consideration of observed values and initial errors in the DA forecast cycle.

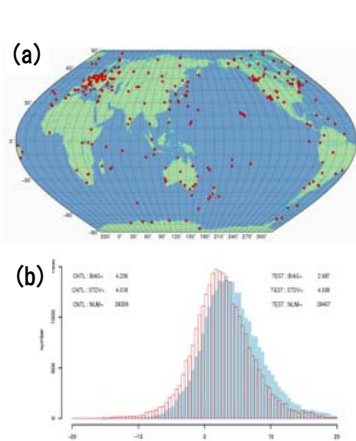


Figure 1. (a) World GPS site map (192 sites, excluding 1,200 sites in Japan), and (b) histograms of PWV O-B (GPS-PWV observations minus forecasts) for TEST (red) and CNTL (blue)

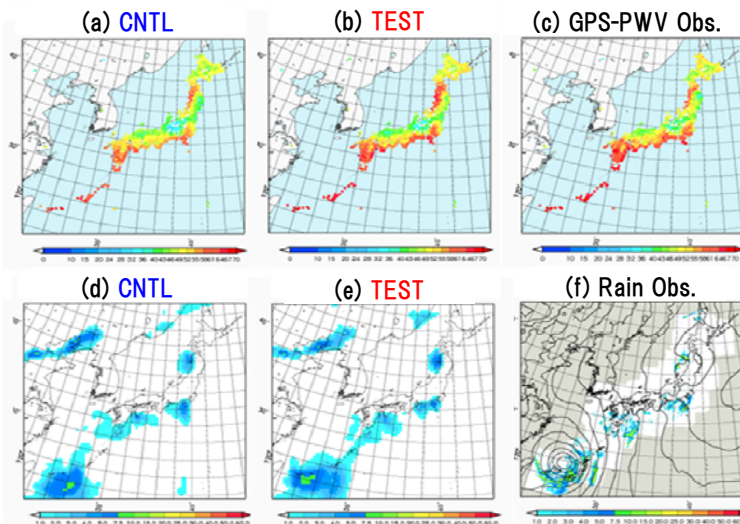


Figure 2. PWV [mm] (top) and rain [mm/hour] (bottom) for observations (c, f) and six-hour forecasts in CNTL (a, d) and TEST (b, e). The PWV observation in (c) was based on data from around 1,200 ground-based GPS sites throughout Japan. The rain observation in (d) was based on data from radar and ground observations in Japan.

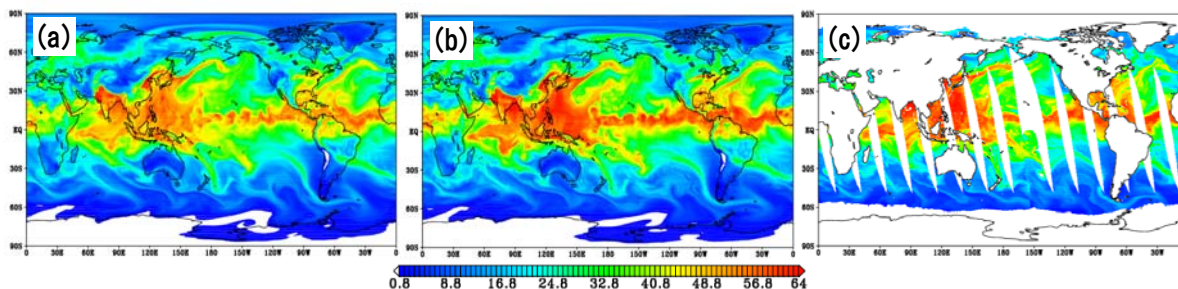


Figure 3. Global PWV fields of three-day forecasts in (a) the CNTL forecast from the CNTL analysis, (b) the TEST forecast from the TEST analysis, and (c) retrieved data from the AMSR-E satellite.

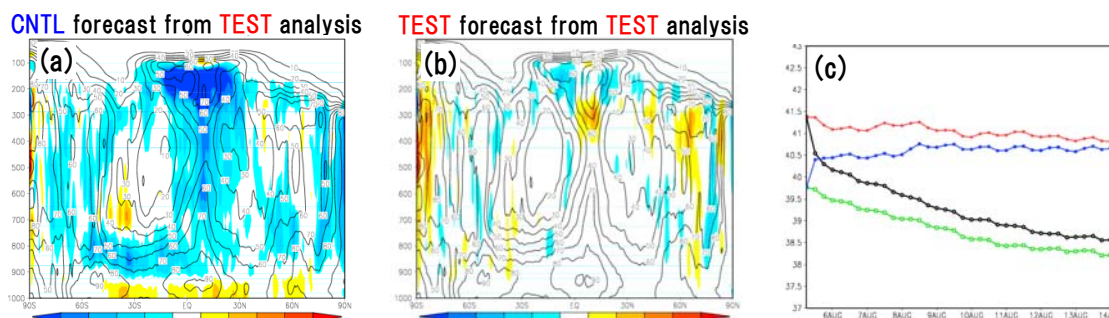


Figure 4. Zonal mean of 24-hour RH change from the initial conditions in (a) the CNTL forecast from the TEST analysis, and (b) the TEST forecast from the TEST analysis. (c) Nine-day PWV forecasts averaged over the tropics (20°S – 20°N) in the TEST forecast from the TEST analysis (red line), the CNTL forecast from the TEST analysis (black line), the TEST forecast from the CNTL analysis (blue line) and the CNTL forecast from the CNTL analysis (green line).

ACKNOWLEDGEMENTS

The GPS observation data (RINEX) is provided by International Global Navigation Satellite System Service (IGS) and Geospatial Information Authority of Japan (GSI). We used GIPSY/OASIS II software package for GPS analysis, which is provided by JPL/NASA.

REFERENCES

Andersson, E., P. Bauer, A. Beljaars, F. Chevallier, E. Holm, M. Janiskova, P. Kallberg, G. Kelly, P. Lopez, A. McNally, E. Moreau, A. Simmons, J.-N. Thepaut, and A. Tompkins, 2005: Assimilation and Modeling of the Atmospheric Hydrological Cycle in the ECMWF Forecasting System. *Bull. Amer. Meteor. Soc.*, **86**, 387–402.

The Problem of Cloud Overlap in the Radiation Process of JMA's Global NWP Model

Ryoji Nagasawa
Climate Prediction Division, Japan Meteorological Agency
1-3-4 Otemachi, Chiyoda-ku, Tokyo 100-8122, Japan
E-mail: r-nagasawa@met.kishou.go.jp

1. Introduction

JMA's global NWP model (JMA-GSM) tends to produce optically thicker (thinner) values in the tropics (extratropics) for shortwave radiation compared with observed values (Fig. 1). One cause of this is insufficient treatment of cloud overlap in shortwave radiation calculation. Against this background, the problem was studied with the aim of improving the treatment.

2. The problem of current cloud overlap in shortwave radiation calculation

In the shortwave radiation scheme of JMA-GSM, the total cloud fraction is calculated with the assumption of a maximum-random overlap with a column area as clear sky and cloudy areas treated separately. In the cloudy area of the column, a random overlap is always adopted to account for cloud multiple scattering effects. In longwave radiation calculation, a maximum-random overlap is adopted (NPD/JMA 2007). If the fraction of optically thin high-level clouds (anvil) is large and that of tower-shaped cumulus clouds is small, which is often observed in the tropics, cloud optical thickness is overestimated in shortwave radiation calculation.

3. The solution

Independent column approximation (ICA, e.g., Cahalan et al. 1994) allows cloud multiple scattering effects to be taken into account in shortwave radiation calculation. This makes it possible to mitigate the aforementioned problem and adopt maximum-random overlap in both shortwave and longwave radiation calculation. Full ICA involves greater computational cost than the current scheme, but Collins (2001) proposed an efficient method called practical ICA (PICA) that involves less accuracy degradation in radiation computation. Essence of the PICA is to ignore radiation calculation in sub-columns whose contribution is small (i.e., narrow columns).

4. Results

Figures 2 and 3 show the impacts of PICA with maximum-random overlap on JMA-GSM and simulated cloud distribution. The approach reduces cloud optical thickness around the tropics and the mid-latitudes (Fig. 2), lowers shortwave heating in the middle troposphere and increases that in the lower troposphere (Fig. 3). The reduced excess shortwave radiation flux reflection in the middle troposphere induces an increase in the downward shortwave radiation flux to the lower troposphere and shortwave radiation absorption by cloud and water vapor below 900 hPa. The PICA method needs to be tested with a variety of cases, and appropriate parameters need to be fixed in consideration of computational cost and accuracy.

References

- Cahalan, R. F., W. Ridgway, W. J. Wiscombe, S. Gollmer and Harshvardhan, 1994: Independent pixel and Monte Carlo estimates of stratocumulus albedo. *J. Atmos. Sci.*, **51**, 3776 – 3790.
- Collins, W. D., 2001: Parameterization of Generalized Cloud Overlap for Radiative Calculation in General Circulation Models. *J. Atmos. Sci.*, **58**, 3224 – 3242.
- Numerical Prediction Division, Japan Meteorological Agency, 2007: Outline of the operational numerical weather prediction at the Japan Meteorological Agency, p. 194.
Available online at <http://www.jma.go.jp/jma/eng/jma-center/nwp/outline-nwp/index.htm>

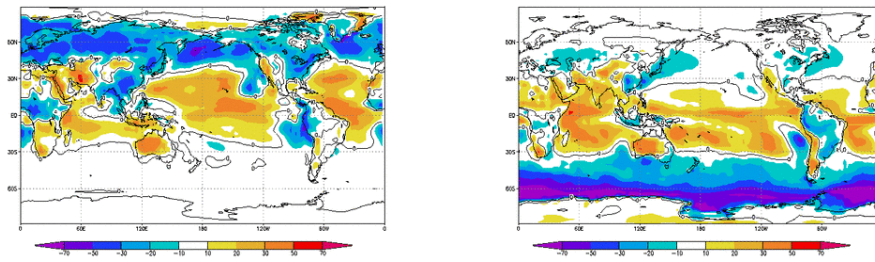


Fig. 1 Upward shortwave radiation flux at TOA (JMA-GSM – CERES) (Wm^{-2}). Left: JJA; right: DJF. The 2001 – 2006 average is shown.

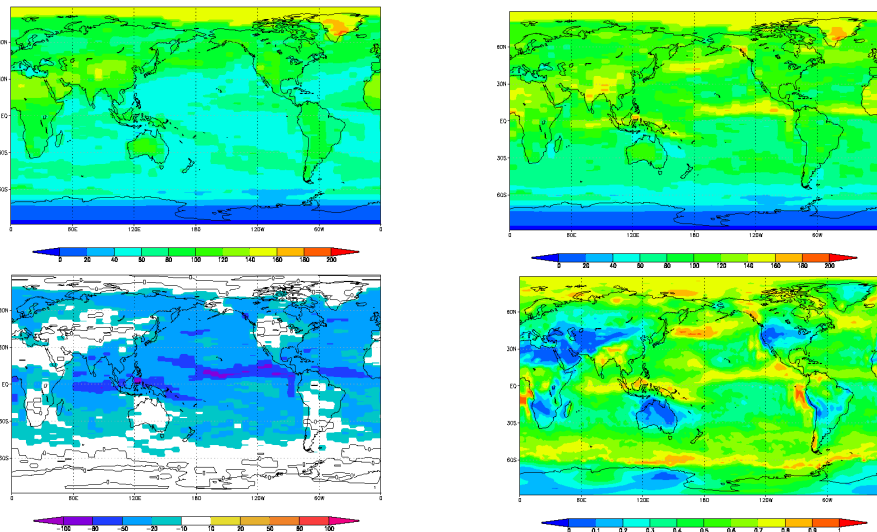


Fig. 2 Impact of difference in cloud overlap assumption for upward shortwave radiation flux at TOA (Wm^{-2}). Upper left: TEST; upper right: CNTL; lower left: TEST – CNTL; lower right: total cloud fraction. The initial time is 12 UTC on 10 August, 2009. The one-month forecast average is shown.

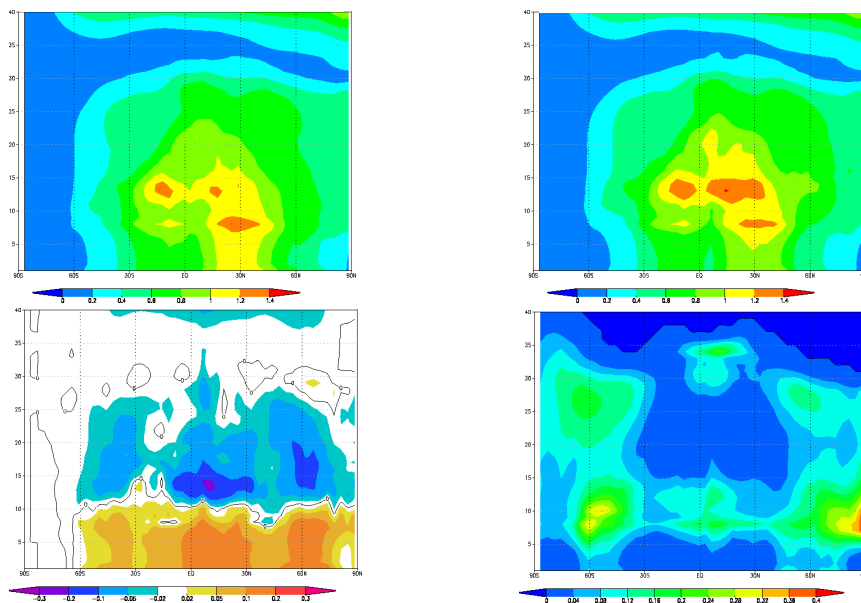


Fig.3 Impact of difference in cloud overlap assumption for the shortwave radiation heating rate (K/day). Upper left: TEST; upper right: CNTL; lower left: TEST – CNTL; lower right: cloud fraction. The initial time is 12 UTC on 10 August, 2009. The zonal mean and the one-month forecast average are shown.

Improvement of the Stratocumulus Parameterization Scheme in JMA's Operational Global Spectral Model

Akira SHIMOKOBE
Numerical Prediction Division, Japan Meteorological Agency
Email: shimokobe@met.kishou.go.jp

1. Introduction and objectives

In JMA's operational global analysis, a negative analysis increment in SLP (sea level pressure) is often seen around North America for 00UTC (Fig. 1). This increment is given by radiosonde temperature observations. Monitoring of cloud cover over this area has shown that the stratocumulus scheme (Kawai and Inoue, 2006) of the Global Spectral Model (GSM) creates afternoon pseudo-clouds, which causes the model's temperature to fall below the observation value in the lower troposphere.

This stratocumulus scheme is designed to represent subtropical marine stratocumulus clouds off the west coast mainly as a function of inversion strength. However, it has been revealed that the scheme works even in dry conditions, which causes the appearance of the pseudo-clouds and the low temperature bias. Accordingly, JMA added a new relative humidity threshold to the conditions in which the scheme works to reduce the occurrence of pseudo-clouds over the continent.

In this report, the operational GSM is referred to as CNTL, and the GSM with the modified stratocumulus scheme is referred to as TEST.

2. Evaluation for North America

Figures 2, 3 and 4 show the results of a TI319 analysis/forecast cycle experiment (low resolution version of the operational global data assimilation system) in October 2010 for North America. Figure 2 shows that there is pseudo-cloud in CNTL in comparison with the visible image for GOES-WEST, but the stratocumulus scheme modification in TEST reduced the amount over North America. Figure 3 shows temperature differences at 850 hPa between radiosonde observations and the first guess of the GSM. For CNTL, the radiosonde temperature observations in the lower troposphere are higher than the model temperatures, but for TEST the model temperatures are close to the observation values. Figure 4 shows the monthly average analysis increment of SLP. For CNTL, negative values are seen for North America, but the negative analysis increment decreases for TEST.

Figure 5 shows a scatter plot of downwelling solar radiation at Fort Peck between the observation and the GSM forecast from 12 UTC October 1st to 12 UTC November 1st. For CNTL, it can be seen that the downwelling shortwave radiation of the GSM forecast is statistically much smaller than that of the observation. However, the GSM forecast for TEST resembles the observation values due to the reduction of pseudo-cloud. The definition of downwelling solar radiation in the GSM forecast differs slightly from that of observation, but its effect is much smaller than the difference between CNTL and TEST.

3. Global evaluation

Figures 6 and 7 also show the results of a TI319 analysis/forecast cycle experiment in October 2010. Figure 6 shows the mean error (ME) and root mean square error (RMSE) of temperature at 850 hPa for a two-day forecast against the values for radiosonde observation. It can be seen that the negative ME bias is alleviated and the RMSE decreased. Figure 7 shows the rate of improvement defined by $(RMSE_{\text{cntl}} - RMSE_{\text{test}}) / RMSE_{\text{cntl}}$. Positive growth is observed, especially in temperature at 850 hPa.

4. Summary

Adding a new relative humidity threshold to the stratocumulus scheme of the GSM reduces the appearance of pseudo-cloud over North America, and this leads to a reduction in the SLP analysis increment. Excess low cloud cover over the continent was found from daily analysis increment monitoring, which is considered effective in improving moist processes in numerical models.

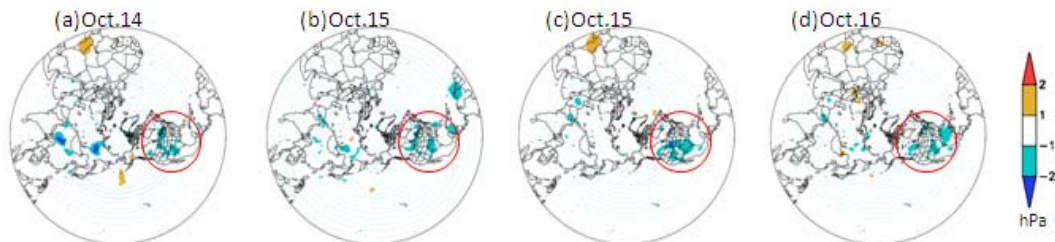


Fig. 1 SLP analysis increment in the JMA's operational global data assimilation system at 00 UTC from (a) October 14 to (d) October 16, 2011

Fig. 2 (a) Visible image of GOES-WEST, and simulated visible cloud images of the GSM for (b) CNTL and (c) TEST at 18 UTC on 14 October 2010

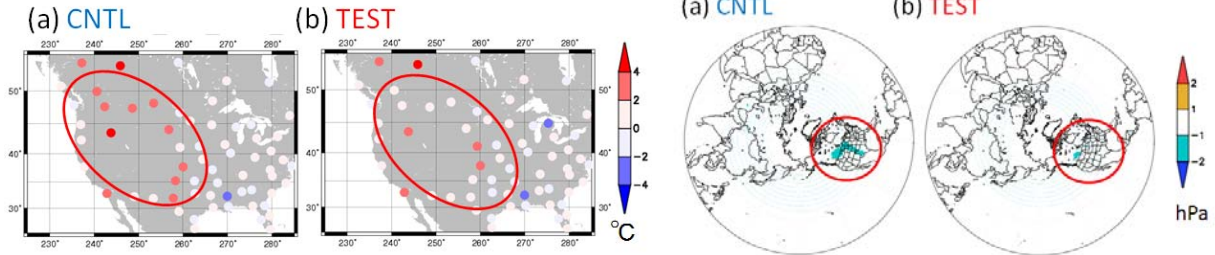
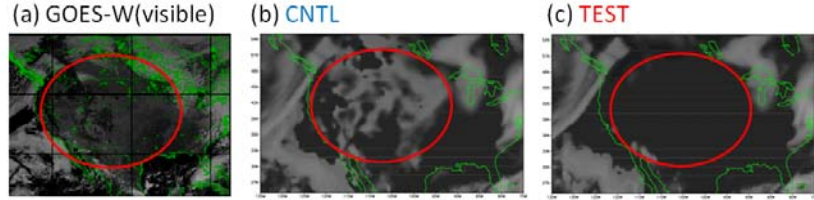


Fig. 3 Temperature differences at 850 hPa between radiosonde observations and the first guess of the GSM at 00 UTC October 15, 2010 for (a) CNTL and (b) TEST.

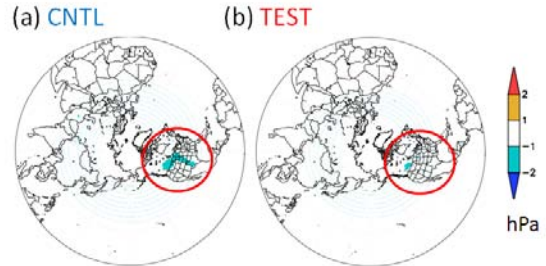


Fig. 4 Average monthly SLP analysis increment at 00 UTC in October 2010 for (a) CNTL and (b) TEST.

Fig. 5 Scatter plot showing downwelling solar radiation [W/m^2] at Fort Peck between the observation (horizontal axis) and the GSM forecast (vertical axis) for (a) CNTL and (b) TEST

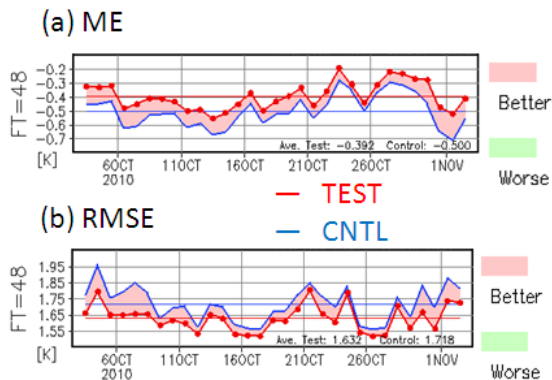
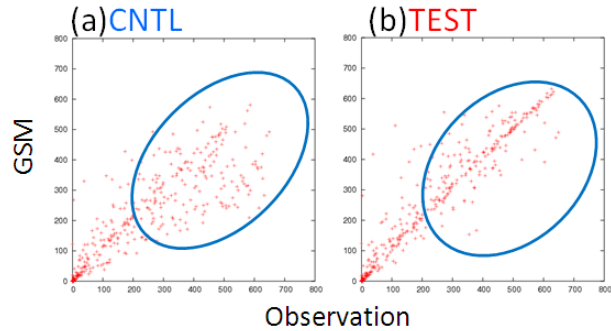


Fig. 6 Verification of temperature at 850 hPa for a two-day forecast against radiosonde observations. (a) ME and (b) RMSE

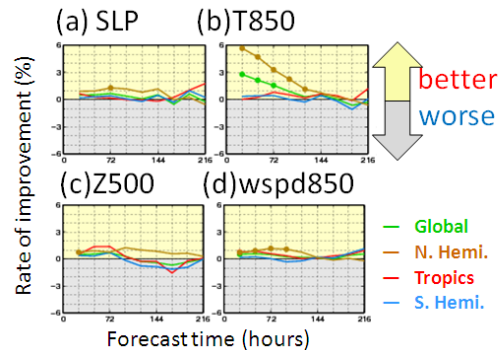


Fig. 7 Verification against the analysis (rate of improvement)

References

Kawai, H. and T. Inoue, 2006: A simple parameterization scheme for subtropical marine stratocumulus. *SOLA*, 2, 17–20.

Acknowledgement

The GOES-WEST image is from the geostationary satellite dataset of the Center for Environmental Remote Sensing at Chiba University. This dataset is supported by the Virtual Laboratory for the Earth's Climate Diagnostics project with funding from Japan's Ministry of Education, Culture, Sports, Science and Technology.

The downwelling solar data for Fort Peck are reproduced courtesy of the SURFRAD project.